Biosensors and Bioelectronics 30 (2011) 287–293

Contents lists available at SciVerse ScienceDirect

Biosensors and Bioelectronics

journal homepage: www.elsevier.com/locate/bios

Mediator-free electrochemical biosensor based on buckypaper with enhanced stability and sensitivity for glucose detection

Asieh Ahmadalinezhad, Guosheng Wu, Aicheng Chen*

Department of Chemistry, Lakehead University, 955 Oliver Road, Thunder Bay, Ontario P7B 5E1, Canada

ARTICLE INFO

Article history:
Received 15 August 2011
Received in revised form
22 September 2011
Accepted 23 September 2011
Available online 1 October 2011

Keywords:
Buckypaper
Biosensor
Mediator-free
Glucose oxidase
Glucose

ABSTRACT

Here we report on a novel platform based on buckypaper for the design of high-performance electrochemical biosensors. Using glucose oxidase as a model enzyme, we constructed a biocompatible mediator-free biosensor and studied the potential effect of the buckypaper on the stability of the biosensor with both amperometry and FTIR spectroscopy. The results showed that the biosensor responses sensitively and selectively to glucose with a considerable functional lifetime of over 80 days. The fabricated enzymatic sensor detects glucose with a dynamic linear range of over 9 mM and a detection limit of 0.01 mM. To examine the efficiency of enzyme immobilization, the Michaelis–Menten constant (K_M^{app}) was calculated to be 4.67 mM. In addition, the fabricated electrochemical biosensor shows high selectivity; no amperometric response to the common interference species such as ascorbic acid, uric acid and acetamidophenol was observed. The facile and robust buckypaper-based platform proposed in this study opens the door for the design of high-performance electrochemical biosensors for medical diagnostics and environmental monitoring.

1. Introduction

Buckypapers are thin membranes (10–50 μm) of carbon nanotube (CNT) networks which are classified as smart nanomaterials owing to their remarkable structural, mechanical, electrochemical, piezoresistive and physical properties (Kang et al., 2006). Since the discovery of CNTs in 1991(Iijima, 1991), tremendous efforts have been made to modify the characteristics of CNTs both chemically (Hrapovic et al., 2004; Kwon et al., 2010; Meng et al., 2009; Zhu et al., 2008) and physically (Wang et al., 2004b) toward the development of thin films of CNTs. Between the two types of CNTs, single-wall carbon nanotubes (SWNTs) and multi-wall carbon nanotubes (MWNTs), SWNTs consist of a single fullerene-structured graphite sheet, which is rolled seamlessly to form a nanotube (Iijima, 1991). SWNTs have a strong tendency to form bundles and aggregate due to their inherently high surface areas and strong Van der Waals interactions. In addition, SWNT networks exhibit higher conductivity than MWNTs (Collins et al., 1997). In addition, mechanical deformation and chemical functionalization can improve interconnectivity of CNTs (Meng et al., 2009). In this regard, polymerization has been widely used in the synthesis of homogenous and compressed CNT films (Ma et al., 2008; Zengin et al., 2002). Park et al. attempted an in situ polymerization method with the aim of dispersing as-pristine SWNT bundles into polyimide with the aid of sonication (Park et al., 2002). Two challenges were encountered: the dispersion issue and the rapidly increasing viscosity of the polymer. This chemical modification may also destroy the pristine structure of the SWNTs, resulting in a decrease of the maximum modulus and strength by 15% (Garg and Sinnott, 1998). Hence, to adapt CNT powder in the formation of substrates for certain applications such as biosensors, a variety of conductive supporting chemical matrices have been explored (Azamian et al., 2002; Chu et al., 2007; Deng et al., 2010; Li et al., 2009a,b; Liu et al., 2005; Rakhi et al., 2009; Rubianes and Rivas, 2009; Tsai et al., 2005; Wang et al., 2004a). Another approach was the introduction of functionalities such as carboxylic groups into the side walls of CNTs. For most of the aforementioned CNT-based sensors, glassy carbon was used as a conductive substrate; however, the fabrication suffered from the necessity of complex reagents, homogeneity and a multiple step preparation process, which in turn, lowered the activity and stability of the resulting sensors.

It has been reported that CNTs in conjunction with a mediator or at a fairly high operating electrode potential have an enhanced effect on the electrocatalytic activity of glucose oxidase (GO_x) for the oxidation of glucose (Cai and Chen, 2004; Deng et al., 2008; Liu et al., 2008, 2005; Rakhi et al., 2009; Zhu et al., 2006). However, mediated biosensors are subjected to a low selectivity and high toxicity. These drawbacks limit their in vivo applications. On the other hand, at a high potential, common electroactive species such as ascorbic acid, uric acid and acetamidophenol may act as interfering agents. Several strategies have been employed to minimize the effects of this interference. Polymeric membranes and

* Corresponding author. Fax: +1 807 3467775.
E-mail address: aicheng.chen@lakeheadu.ca (A. Chen).

0956-5663/$ – see front matter © 2011 Elsevier B.V. All rights reserved.
doi:10.1016/j.bios.2011.09.030

metal-based compounds have been utilized (Ahmadalinezhad et al., 2009; Benvenuto et al., 2009; Newman et al., 1995; Tsai et al., 2005; Wang, 2008). Effective but nonsufficient rejection of interferents has been reported in most cases. Moreover, multiple preparation steps and manipulation lower the sensor activity and increase its complexity. Such detection relies on the tuning of the operating potential to the optimal region of 0.0 to −0.20 V vs Ag/AgCl to effectively detect hydrogen peroxide released from the reaction of GO_x and glucose using peroxidases (Wang, 2008). Although a few mediator-free bi-enzyme glucose sensors based on CNTs have been reported in the literature (Gu et al., 2010; Yao and Shiu, 2008; Zeng et al., 2007; Zhu et al., 2007), the narrow linear dynamic range, low sensitivity and stability hamper their medical diagnostic application.

In this study, we have designed a mediator-free glucose sensor based on buckypaper. To the best of our knowledge, this is the first time that titanium interfaced buckypaper has been explored in the design of an electrochemical biosensor. Titanium was chosen as the substrate because of its good conductivity, biocompatibility and high corrosion resistance. The glucose sensor fabricated with the scheme proposed in this study exhibited high sensitivity, stability, selectivity and reproducibility. The robust buckypaper-based platform presented in this study is anticipated to open the door for the design of high-performance electrochemical biosensors for medical diagnostics and environmental monitoring.

2. Experimental

2.1. Reagents and materials

The buckypaper used in this study was produced by the High-Performance Materials Institute of Florida State University with a thickness of 0.035 mm. Glucose oxidase (EC 1.1.3.4, Type VII from *Aspergillus niger*) and β-D-glucose were purchased from Sigma and were used as received. Chitosan was purchased from Aldrich and titanium foils (99.2%) from Alfa Aesar. Horseradish peroxidase (HRP), potassium ferricyanide ($K_3Fe(CN)_6$), ascorbic acid, uric acid, 3-acetamidophenol were purchased from Sigma–Aldrich. All other reagents were of analytical grade. Water was purified with the Nanopure® water system (18 MΩ cm) and was used in the preparation of all solutions. Various stock concentrations of β-D-glucose were prepared in 0.1 M phosphate buffer, pH 7.4 and stored at 4 °C. Glucose stock solutions were allowed to mutarotate overnight prior to use.

2.2. Instrumentation and electrochemical measurements

Field-emission scanning electron microscopy (FE-SEM) (Hitachi, SU-4800), transmission electron microscopy (TEM) (JOEL 2010F) and energy dispersive X-ray spectrometry (EDS) were utilized to characterize the morphology and composition of the buckypaper. FTIR spectra were recorded using a NICOLET 8700 FTIR (Thermo Scientific, USA). Cyclic voltammetry (CV) and amperometric measurements were performed using an electrochemical workstation (CHI660, CH Instrument Inc., USA) connected with an in-house-built, three-electrode glass cell (30 mL). A platinum coil was used as a counter electrode and was flame-annealed prior to each experiment. Ag/AgCl (3 M KCl) was used as a reference electrode. The constructed hybrid titanium/buckypaper-based biosensors were employed as working electrodes. All measurements were conducted at room temperature (22 ± 2 °C).

2.3. Biosensor preparation

The detailed procedure of the biosensor fabrication is illustrated in Fig. 1. Titanium plates (1.25 cm × 0.8 cm × 0.5 mm) were ultrasonically cleaned in acetone, ethanol and water. To provide a mechanical support for the buckypaper and to enhance the conductivity, a titanium plate was coated with an Au thin film sputtered by argon plasma for 30 s (Fig. 1a). After rinsing with pure water, a section of buckypaper was attached to the gold coated titanium plate with the aid of 5 μL of 2 mg mL^{-1} chitosan (Fig. 1b and c). In order to engender this structure with utility as a glucose biosensor, the buckypaper was electrochemically activated. To activate the buckypaper (BP) surface, cyclic voltammetry was performed in the range of −0.8 to 0.4 V at a scan rate of 10 mV s^{-1} in a phosphate buffer solution (PBS) at pH 7.4 until a steady cyclic voltammogram was obtained, and then a potential of 1.5 V was applied for 90 s. This step led to the functionalization of the buckypaper with carboxlic groups (Fig. 1d). The activated surface was thus ready for the immobilization of enzymes. To immobilize the enzymes, a mixed solution of 20 μL of 5 mg mL^{-1} GO_x, 10 μL of 2 mg mL^{-1} HRP and 10 μL of 2 mg mL^{-1} chitosan was cast onto the buckypaper (Fig. 1e and f). All prepared biosensors (Ti/Au/BP/GO_x-HRP) were stored at 4 °C in 0.1 M PBS at pH 7.4 when not in use.

2.4. Surface morphological studies

The morphology and composition of the buckypaper were characterized using FESEM, TEM and EDS. Fig. 2a shows a photograph of the buckypaper used in this study. It is a very thin film. A typical FESEM image is presented in Fig. 2b, which reveals that the SWNTs were arranged in bundles, forming networks. A high magnification TEM image of the buckypaper is displayed in Fig. 2c, showing that the nanotubes were aggregated in a rope structure; the diameter of an individual SWNT was less than 4 nm. The volume density of buckypaper represents a high specific surface area, desirable for the immobilization of enzymes. Fig. 2d shows the EDS spectrum of the buckypaper. Only carbon and oxygen peaks were observed with no other discernable peaks, indicating the absence of impurities such as heavy metals.

2.5. Electrochemical characterization

The cyclic voltammograms of the Ti/BP, Ti/Au/BP, and Ti/Au/BP/GO_x-HRP electrodes recorded in 0.1 M $K_3Fe(CN)_6$ + 0.1 M KCl + 0.1 M PBS (pH 7.4) at a scan rate of 50 mV s^{-1} are presented in Fig. 3A. The well-defined oxidation and reduction peaks are observable due to the Fe^{3+}/Fe^{2+} redox couple. In the absence of the Au thin film, the oxidation peak appeared at 0.46 V, while the reduction peak was observed at around −0.36 V vs Ag/AgCl. The peak-to-peak separation (ΔE_p) was 0.82 V for the Ti/BP electrode. While in the presence of the sputtered Au thin film (Ti/Au/BP electrode), ΔE_p decreases to 0.47 V. In addition, the peak current increased by approximately 40%. All these results show that the sputtered gold thin film significantly enhanced the electrical communication between the buckyppaer and the titanium substrate. After the immobilization of the enzymes GO_x and HRP, both ΔE_p and peak current (I_p) slightly decreased. The electrochemical active surface area of the Ti/Au/BP and Ti/Au/BP/GO_x-HRP electrodes may be calculated via the Randles–Sevcik equation (Bard and Faulkner, 2000):

$$I_p = 2.69 \times 10^5 A D^{1/2} n^{3/2} \upsilon^{1/2} C$$

where n is the number of electrons that participate in the redox reaction, A is the area of the electrode (cm^2), D is the diffusion coefficient of the probe molecule in the bulk solution (cm^2 s^{-1}), C is the concentration of the $K_3Fe(CN)_6$ in the bulk solution (mol cm^{-3}), and υ is the scan rate (V s^{-1}). The electroactive surface area of the Ti/Au/BP and Ti/Au/BP/GO_x-HRP electrodes is thus estimated to be 1.85 and 1.75 cm^2, respectively. The slightly decrease in the

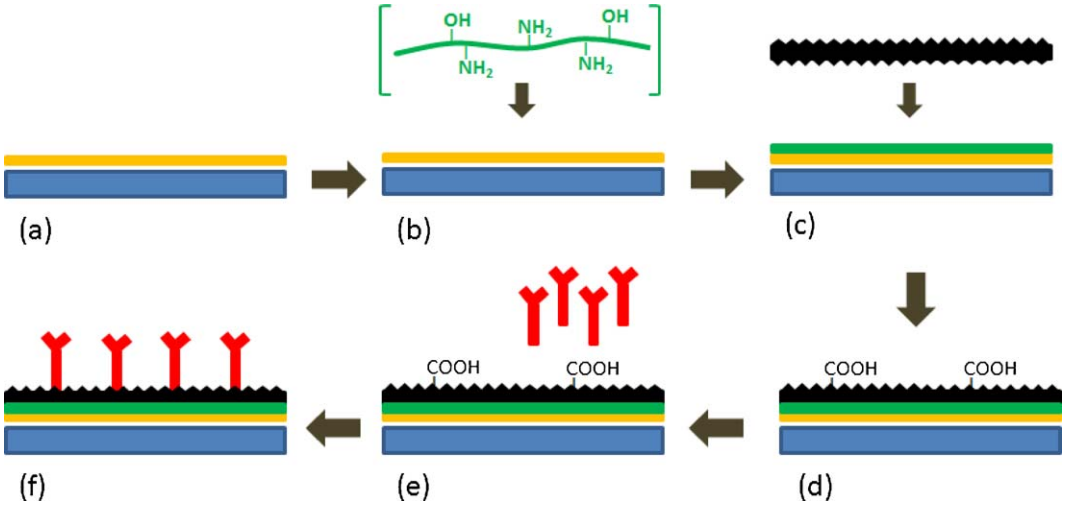

Fig. 1. Schematic diagram for the preparation of the buckypaper-based electrochemical biosensor. (a) A titanium plate sputtered with a thin layer of gold; (b) gold interaction with chitosan; (c) attachment of buckypaper to the gold surface by chitosan; (d) activation of buckypaper; (e) immobilization of enzymes; (f) the fabricated biosensor.

electroactive surface area subsequent to the immobilization of the enzymes can be attributed to the blockage of some redox sites by GO_x and HRP, indicating that the immobilization did not diminish electron transfer between the redox species and the electrode substrate (Fig. 3).

To investigate whether GO_x immobilized on the activated buckypaper retains its bio-electrocatalytic activity for the oxidation of glucose, control experiments were conducted for the Ti/Au/PB, Ti/Au/PB/HRP and Ti/Au/BP/HRP-GO_x electrodes. As seen in the CV curves (Fig. 3B) recorded in 0.1 M PBS (pH 7.4), a pair of well-defined peaks centered at −0.19 and −0.5 V were observed for the Ti/Au/PB electrode, which can be attributed to the surface functionalities of the activated buckypaper. The well-defined peaks disappeared after the immobilization of HRP with the aid of chitosan due to the interactions between the functional groups of the activated buckypaper and chitosan. In contrast, a pair of well-defined redox peaks located at −0.09 and −0.35 V appeared after the co-immobilization of HRP and GO_x with the aid of chitosan, showing the direct electrochemistry of the GO_x immobilized on the buckypaper. The formal potential, $E^0 = 1/2\ (E_{pa} + E_{pc})$, was calculated to be −0.22 V. This indicates that the activated buckypaper improves the contact between the electrode surface and GO_x and decreases the

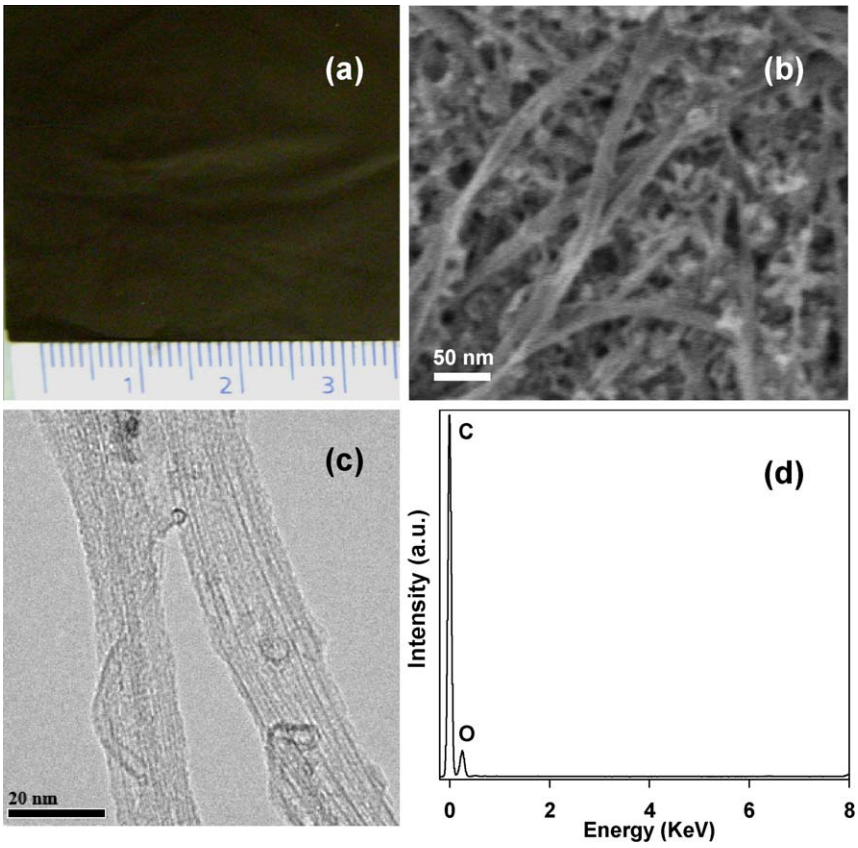

Fig. 2. (a) A photograph; (b) FESEM image; (c) TEM image; and (d) the corresponding EDS spectrum of the buckypaper.

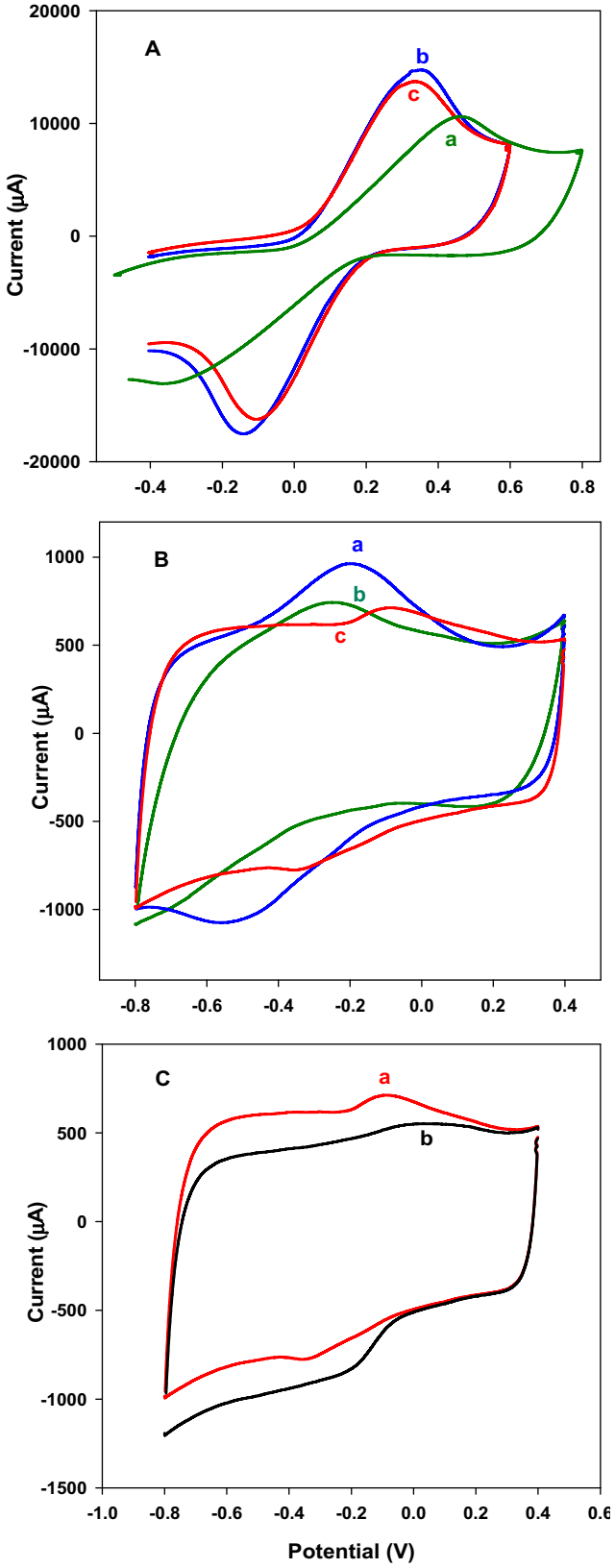

Fig. 3. Cyclic voltammograms of (A) Ti/BP (a), Ti/Au/BP (b), and Ti/Au/BP/GO_x-HRP (c) electrodes at a scan rate of 50 mV s^{-1} in 0.1 M $K_3Fe(CN)_6$ + 0.1 M KCl + PBS solution pH 7.4. (B) Ti/Au/BP (a), Ti/Au/BP/HRP (b), and Ti/Au/BP/GO_x-HRP (c) electrodes, and (C) Ti/Au/BP/GO_x-HRP electrode before (a) and after (b) injection of 10 mM glucose at the scan rate of 10 mV s^{-1} in PBS pH 7.4.

overpotential required for the FAD/$FADH_2$ redox reaction (Wang et al., 2002). The effect of the scan rate on the cyclic voltammograms of the Ti/Au/BP/GO_x-HRP electrode was studied in the range of 5–50 mV s^{-1} in 0.1 M PBS (data not shown). A pair of symmetric and well-defined redox peaks were obtained with a linear relationship between the current and scan rate, indicating that the redox process of the immobilized GO_x is a surface-controlled redox reaction rather than diffusion-controlled reaction. The amount of the electroactive enzymes, $\Gamma = Q/nFA$, (where Q is the charge, n is the electron transfer number, F is the faraday constant, and A is the geometric area of the working electrode) was calculated to be 3.65×10^{-9} mol cm^{-2}. This value is much higher than the theoretical value for a monolayer of GO_x (2.86×10^{-12} mol cm^{-2}) (Xu et al., 2003) and a monolayer of HRP (8.5×10^{-12} mol cm^{-2}) (Liu and Gooding, 2006) and experimental values (7.52×10^{-10} mol cm^{-2} for GO_x and 2.1×10^{-11} mol cm^{-2} for HRP) reported in the literature (Deng et al., 2009, 2010; Huang et al., 2005; Zhao et al., 2008), indicating that the enzymes immobilized on the buckypaper effectively participated in the electron transfer.

We further studied the response of the Ti/Au/BP/GO_x-HRP electrode to glucose. As shown in Fig. 3C, upon addition of 10 mM glucose, the oxidation peak current decreased while the reduction current significantly increased, showing a strong response to glucose. This can be attributed to the reduction of H_2O_2 generated by the oxidation of glucose by the immobilized GO_x as per the following equations (Liu et al., 2005; Reilly and Aust, 1997; Rodriguez-Lopez et al., 2001)

$$\beta\text{-d-glucose} + GO_x\text{-FAD} \rightarrow \delta\text{-d-gluconolactone} + GO_x\text{-}FADH_2 \quad (1)$$

$$GO_x\text{-}FADH_2 + O_2 \rightarrow GO_x\text{-FAD} + H_2O_2 \quad (2)$$

$$HRP(Fe^{3+}) + H_2O_2 \rightarrow \text{Compound I}(Fe^{4+} = O) + H_2O \quad (3)$$

$$\text{Compound I}(Fe^{4+} = O) + e^- + H^+ \rightarrow \text{Compound II} \quad (4)$$

$$\text{CompoundII} + e^- + H^+ \rightarrow HRP(Fe^{3+}) + H_2O \quad (5)$$

GO_x, as a glycoprotein, oxidizes glucose to gluconolactone and hydrogen peroxide in the presence of oxygen. On the other hand, HRP, as an oxidative heme-containing enzyme, cleaves the O–O bond of hydrogen peroxide. Compound I is an intermediate comprising a ferryl species and a porphyrin radical cation; while Compound II is the second intermediate from the first reduction of the porphyrin radical cation, which retains the heme in the ferryl state.

To achieve a maximum current response, the detection of glucose under optimized applied potential is necessary. Fig. S1A (see Supplementary data) shows the responses of the Ti/Au/BP/GO_x-HRP biosensor upon the successive addition of 2 mM glucose at different potentials. At 0.1 V a small current response was observed. The cathodic current response to glucose significantly increased when the potential was lowered to −0.1 V. By further lowering the electrode potential to −0.2 or −0.3 V, the current response decreased. Fig. S1B compares the corresponding current response to 4 mM glucose at different potentials, showing that −0.1 V is the optimum potential for the Ti/Au/BP/GO_x-HRP biosensor.

The amperometric response of the Ti/Au/BP/GO_x-HRP biosensor at the optimized potential under the physiological pH 7.4 upon the successive addition of 1 mM glucose is shown in Fig. 4. For comparison, the amperometric response of the Ti/Au/BP electrode is also included in Fig. 4A. No obvious current response was observed at the non-enzymatic electrode, while a strong response was achieved by the enzymatic electrode. Fig. 4B shows the corresponding current vs glucose concentration plot for the biosensor. A

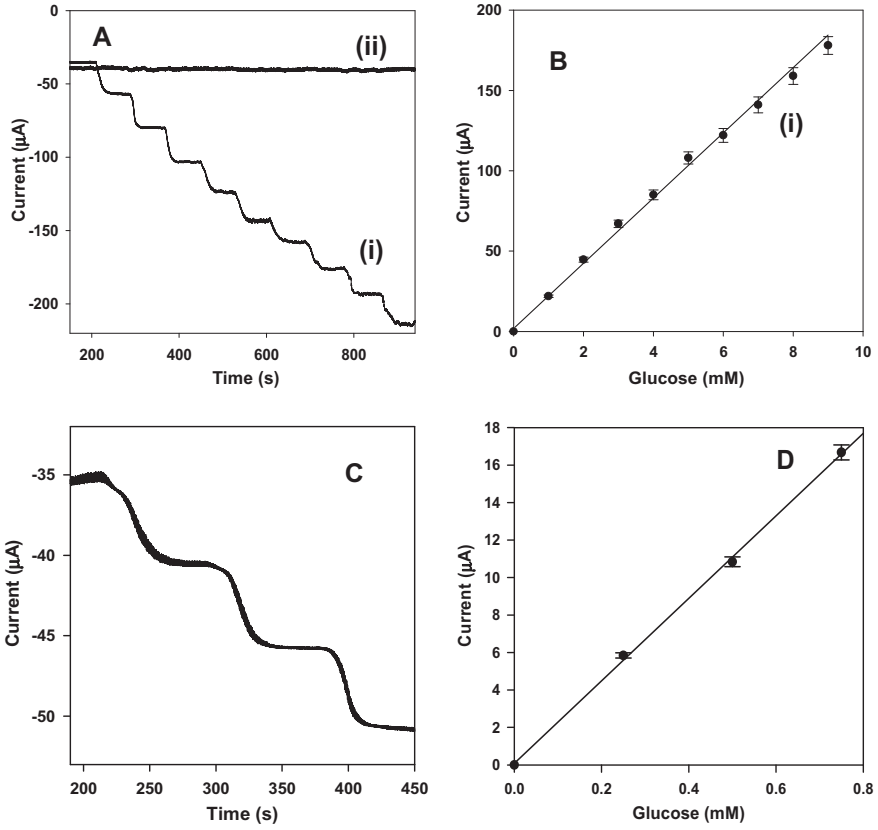

Fig. 4. Amperometric response and calibration curve of the Ti/Au/BP/GO_x-HRP (i) and Ti/Au/BP (ii) electrodes upon addition of 1 mM glucose (A and B) and of the Ti/Au/BP/GO_x-HRP upon addition of 0.25 mM (C and D) at −0.1 V in PBS pH 7.4.

linear relationship with a correlation coefficient R^2 of 0.993 was obtained in the glucose range of over 9 mM, which effectively covers the normal physiological glucose range (3–7 mM). The sensitivity and the detection limit of the fabricated biosensor are thus estimated to be 20 μA mM^{-1} cm^{-2} and 0.01 mM, respectively. To examine the ability of the biosensor to detect low concentrations of glucose, the amperometric study was further conducted with the injection of 0.25 mM glucose under the same experimental conditions. As shown in Fig. 4C, a strong response to each injection was observed. A linear relationship with a correlation coefficient R^2 of 0.993 (Fig. 4D) was obtained in the range of 0–0.75 mM glucose; and the relative standard deviation (RSD) was estimated to be 2.4%. The calculated sensitivity is as high as the one determined from Fig. 4B for the 1 mM successive injection, further showing that the biosensor is very sensitive to glucose (Fig. 4).

To evaluate the efficiency of the immobilized enzymes, the apparent Michaelis–Menten constant, (K_M^{app}) can be determined using the following "Lineweaver–Burk" type equation:.

$$\frac{1}{I_{ss}} = \left(\frac{K_M^{app}}{I_{max}}\right)\left(\frac{1}{C}\right) + \frac{1}{I_{max}}$$

where I_{max} and I_{ss} are the currents measured for enzymatic product detection under conditions of substrate saturation and steady state, respectively, for a given substrate concentration C (Kamin and Wilson, 1980; Shu and Wilson, 1976). This equation allows us to plot the experimental I_{max}/I_{ss} vs $1/C$ to determine K_M^{app} from the slope of the resultant linear plot. The value of K_M^{app} was obtained to be 4.67 mM for the fabricated biosensor. This low K_M^{app} value reflects the efficient enzyme immobilization process proposed in this study.

2.6. Selectivity of the biosensor

To investigate the selectivity of the Ti/Au/BP/GO_x-HRP biosensor, we tested its response to the common interfering species including ascorbic acid (AA), uric acid (UA) and acetamidophenol (AP). As shown in Fig. S2, there is no salient current response upon the addition of the interferents at their physiological level, 0.1 mM AA, 0.1 mM UA and 0.1 mM AP. In contrast, a strong response to the successive injection of 1 mM glucose was observed in the presence of all the three common interfering species, showing that the Ti/Au/BP/GO_x-HRP biosensor allows for the highly selective quantification of glucose without the usage of membranes or metal particles.

2.7. Stability of the biosensor

The stability of the fabricated biosensor was further investigated. The biosensor was tested once a week in a stirring cell during the electrochemical measurements. It was stored in 0.1 M PBS (pH 7.4) at 4 °C when not in use. Fig. 5A presents the amperometric response of the Ti/Au/BP/GO_x-HRP biosensor at the beginning (red line) and after 80 days (black line) upon addition of 1.2 mM glucose at −0.1 V in 0.1 M PBS (pH 7.4), revealing that the biosensor retained 94% of its initial current response after such a long period of time. Three biosensors were prepared and tested for their stability. Fig. 5B presents the amperometric response of the biosensors versus time. The relative standard deviation of their response to glucose was 3.0%. Over 98% of their initial current response was retained during the first 50 days. The reproducibility of the biosensor for the current response was also tested, showing that the RSD was 3.5% for 10 successive measurements of 1 mM glucose at −0.1 V in 0.1 M PBS (pH 7.4). We further compared the performance

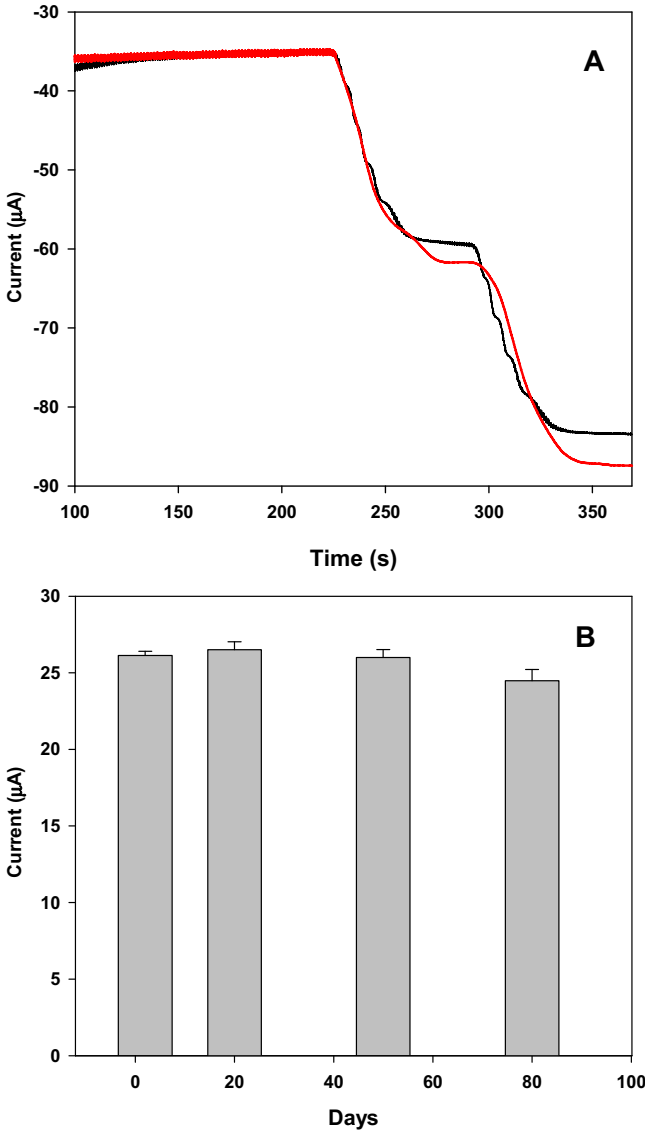

Fig. 5. (A) Amperometric response of the Ti/Au/BP/GO_x-HRP electrode initially (red line) and after a period of 80 days (black line) upon addition of 1.2 mM glucose at −0.1 V in PBS pH 7.4. (B) Comparison of the current response of the Ti/Au/BP/GO_x-HRP electrode to 1.2 mM glucose during the 80-day stability tests. (For interpretation of the references to color in this figure legend, the reader is referred to the web version of the article.)

of the biosensor developed in this study with that of the various CNT-based glucose biosensors reported in the literature. As seen in Table 1, the mediator-free biosensor developed in this study possesses remarkable properties in terms of linear dynamic range and stability compared to the other mediator-based and mediator-less biosensors (Fig. 5).

During the 80-day stability tests, the biosensors were washed each time and the temperature was changed regularly between 4 °C and room temperature. The long lifetime shows that the Ti/Au/BP/GO_x-HRP biosensor fabricated by the innovative procedure proposed in this study possesses high thermal stability and excellent mechanical strength. This can be attributed to the efficient immobilization of the enzymes along with the unique physical and chemical properties of the activated buckypaper. The interaction between the Au thin film sputtered on the Ti substrate and the buckypaper with the aid of chitosan is so strong that it is almost impossible to remove the buckypaper from the substrate without breaking the buckypaper film. Chitosan contains primary amines, hydroxyl and acetyl groups which under weakly acidic conditions are protonated. These charged functional groups on chitosan molecules might induce strong adsorption of chitosan onto the surface of Au in the way similar to the modification of Au surface with charged alkanethiols (Hu and Bard, 1998). To decipher the significant role of the activated buckypaper in the fabrication of the biosensor with high stability, we carried out FTIR analysis. Fig. S3 presents the FTIR spectra of the activated buckypaper (a), chitosan immobilized on the activated buckypaper (b), and chitosan (c). For the activated buckypaper (Fig. S3a), several strong peaks were observed. The peaks located at 1719 and 1652 cm^{-1} can be assigned to the C=O stretching vibration of –COOH and $–COO^-$ groups, respectively, which were generated during the electrochemical treatment. The peaks at 1597, 1505 and 1448 cm^{-1} could be attributed to the C=C aromatic vibrational modes of the SWNTs in accordance with previous reports (Cai and Chen, 2004; Chen et al., 1998; Ortiz et al., 1995). The FTIR spectrum of chitosan (Fig. S3c) contains the C–N stretching at 1404 cm^{-1} and NH_2 bending vibration modes at ~1549 and 1638 cm^{-1}. The upshift in this region observed in the spectrum of the chitosan–buckypaper indicates a strong interaction between the –COOH and $–NH_2$ groups and the formation of –NHCO– (Fig. S3b). The very strong peaks at 1022 and 1062 cm^{-1} are the typical stretching vibration of the C–O bond. The peak at 1638 cm^{-1} in the spectrum of chitosan which can be related to the N–H of amide (I) group, almost disappeared in the spectrum of chitosan–buckypaper. The spectrum of the activated buckypaper shows strong peaks at 1200 and 1263 cm^{-1} which can be attributed to C–O aliphatic group and C–O of carboxylic acids, respectively. These two peaks also disappeared in the spectrum of chitosan–buckypaper. Two bands

Table 1
Comparison of the performance of different carbon nanotube-based glucose biosensors.

Electrode modifier	Detection limit (μM)	Linear range (mM)	Stability	Detection potential (V)	Ref.
(Au-Pt)NPs/CNT/Au/GO_x	400	0.5–17.5	75% (25 days)	0.6	Chu et al. (2007)
GCE/PB/MWNT/GO_x	12.7	0.0–8.0	85% (14 days)	0.0	Zhu et al. (2006)
GCE/CNT-PtNPs/GO_x	0.5	0.5×10^{-3}–5.0	N/A	0.55	Hrapovic et al. (2004)
PDDA/GO_x/PDDA/CNT/GCE	7.0	15×10^{-3}–6.0	90% (30 days)	−0.1	Liu and Lin (2006)
MWNT/Nafion/GCE/GO_x	4.0	25×10^{-3}–2	N/A	0.7	Tsai et al. (2005)
GCE/CNT-CHIT-GDI-GDH	3.0	5×10^{-3}–0.3×10^{-3}	80% (4 days)	0.4	Zhang et al. (2004)
SWNTs/Nafion/GCE/FMCA	6.0	0.0–6.0	N/A	0.3	Liu et al. (2008)
GC/CNT/HRP-GO_x/Nafion	0.5	0.025–0.4	97% (7 days)	0.0	Yao and Shiu (2008)
Au/SWNT/GOD-HRP/PPy	90	0.030–2.43	67% (14 days	−0.1	Zhu et al. (2007)
HRP-GO_xCNT/PAMAM	2.5	0.004–1.2	N/A	−0.34	Zeng et al. (2007)
GOD–HRP–Cys–SG/GNP/ITO	10	0.02–3.2	80% (5days)	−0.1	Gu et al. (2010)
Ti/Au/BP/GO_x-HRP	10	0.0–9.0	94% (>80 days)	−0.1	Proposed biosensor

GCE: glassy carbon electrode, GO_x: glucose oxidase, MWNTs: multi-walled carbon nanotubes, PB: Prussian blue, PDDA: polydiallyldimethylammonium chloride, SWNTs: single-walled carbon nanotubes, Au: gold, PtNPs: Platinum nanoparticles, CNT: carbon nanotubes, CHIT: chitosan, GDI: glutaric dialdehyde, GDH: glucose dehy-drogenase; FMCA: ferrocene monocarboxylic acid; PPy: polypyrrole; PAMAM: poly(amidoamine); Cys: L-Cysteine; SG: sol–gel; ITO: indium tin oxide; N/A: not available.

of the glucopyranose rings appeared at ca. 892 and 1150 cm^{-1}, implying the attachment of chitosan to the activated buckypaper. These results confirm the functionalization of the buckypaper with chitosan, which has strong interactions with nucleophilic substitutions by primary and secondary amines that exist in abundance on the surface of the glycoprotein. Therefore, the interconnectivity of physically aggregated CNTs in the buckypaper, its compatibility and strong interactions with chitosan on one hand and chitosan interaction with the enzymes on the other hand may significantly enhance the interfacial adhesion and mechanical strength of the biosensor.

3. Conclusion

In summary, we have fabricated a mediator-free glucose biosensor based on the co-immobilization of GO_x and HRP on the activated buckypaper. Direct electrochemistry of GO_x on the buckypaper was observed. The glucose biosensor showed a high sensitivity, low detection limit (0.01 mM), fairly wide linear dynamic range (0–9 mM), long life-time (over 80 days) and high selectivity in the presence of common interferent species under the physiological condition. These properties of the buckypaper-based biosensor, coupled with the biocompatibility of its components are important factors which could be attractive for real-time in vivo glucose monitoring and lead to a substantial improvement in the management of diabetes. The facile and robust buckypaper-based platform proposed in this study opens many opportunities for the development of high-performance electrochemical biosensors for medical diagnostics and environmental monitoring.

Acknowledgements

This work was supported by a Discovery Grant from the Natural Sciences and Engineering Research Council of Canada (NSERC). We greatly appreciate the provision of the buckypaper samples by Prof. B. Wang and Prof. Z. Liang of the High-Performance Materials Institute, Florida State University. A.C. acknowledges the NSERC and the Canada Foundation for Innovation (CFI) for the Canada Research Chair Award in Materials & Environmental Chemistry.

Appendix A. Supplementary data

Supplementary data associated with this article can be found, in the online version, at doi:10.1016/j.bios.2011.09.030.

References

Ahmadalinezhad, A., Kafi, A.K.M., Chen, A., 2009. Electrochem. Commun. 11, 2048–2051.
Azamian, B.R., Davis, J.J., Coleman, K.S., Bagshaw, C.B., Green, M.L.H., 2002. J. Am. Chem. Soc. 124, 12664–12665.
Bard, A.J., Faulkner, L.R., 2000. Electrochemical Methods-Fundamentals and Applications. John Wiley and Sons, New York.
Benvenuto, P., Kafi, A.K.M., Chen, A., 2009. J. Electroanal. Chem. 627, 76–81.
Cai, C., Chen, J., 2004. Anal. Biochem. 332, 75–83.
Chen, J., Hamon, M.A., Hu, H., Chen, Y., Rao, A.M., Eklund, P.C., Haddon, R.C., 1998. Science 282, 95–98.
Chu, X., Dua, D., Shen, G., Yu, R., 2007. Talanta 71, 2040–2047.
Collins, P., Zettl, A., Bando, H., Thess, A., Smalley, R., 1997. Science 278, 100–103.
Deng, C., Chen, J., Nie, Z., Si, S., 2010. Biosens. Bioelectron. 26, 213–219.
Deng, L., Wang, Y., Shang, L., Wen, D., Wang, F., Dong, S., 2008. Biosens. Bioelectron. 24, 951–957.
Deng, S., Jian, G., Lei, J., Hu, Z., Ju, H., 2009. Biosens. Bioelectron. 25, 373–377.
Garg, A., Sinnott, S., 1998. Chem. Phys. Lett. 295, 273–280.
Gu, M., Wang, J., Tu, Y., Di, J., 2010. Sens. Actuators B: Chem. 148, 486–491.
Hrapovic, S., Liu, Y., Male, K.B., Luong, J.H.T., 2004. Anal. Chem. 76, 1083–1088.
Hu, K., Bard, A.J., 1998. Langmuir 14, 4790–4794.
Huang, Y., Zhang, W., Han Xiao, G.L., 2005. Biosens. Bioelectron. 21, 817–821.
Iijima, S., 1991. Nature 354, 56–58.
Xu, J.Z., Zhu, J.J., Wu, Q., Hu, Z., Chen, H.Y., 2003. Chin. J. Chem. 21, 1088–1091.
Kamin, R.A., Wilson, G.S., 1980. Anal. Chem. 52, 1198–1205.
Kang, I., Schulz, M.J., Kim, J.H., Shanov, V., Shi, D., 2006. Smart Mater. Struct. 15, 737–748.
Kwon, K.Y., Yang, S.B., Kong, B.-S., Kim, J., Jung, H.-T., 2010. Carbon 48, 4504–4509.
Li, F., Song, J., Li, F., Wang, X., Zhang, Q., Han, D., Ivaska, A., Niu, L., 2009a. Biosens. Bioelectron. 25, 883–888.
Li, F., Wang, Z., Shan, C., Song, J., Han, D., Niu, L., 2009b. Biosens. Bioelectron. 24, 1765–1770.
Liu, G., Gooding, J.J., 2006. Langmuir 22, 7421–7430.
Liu, G., Lin, Y., 2006. Electrochem. Commun. 8, 251–256.
Liu, X., Shi, L., Niu, W., Li, H., Xu, G., 2008. Biosens. Bioelectron. 23, 1887–1890.
Liu, Y., Wang, M., Zhao, F., Xu, Z., Dong, S., 2005. Biosens. Bioelectron. 21, 984–988.
Ma, Y., Cheung, W., Wei, D., Bogozi, A., Chiu, P.L., Wang, L., Pontoriero, F., Mendelsohn, R., He, H.X., 2008. ACS Nano 2, 1197–1204.
Meng, C., Liu, C., Fan, S., 2009. Electrochem. Commun. 11, 186–189.
Newman, J.D., White, S.F., Tothill, I.E., Tumer, A.P.F., 1995. Anal. Chem. 67, 4594–4600.
Ortiz, R., Mfirquez, O.P., Mfirquez, J., Guti, rez, C, 1995. J. Electroanal. Chem. 390, 99–107.
Park, C., Ounaies, Z., Watson, K., Crooks, R., Smith, J.J., Lowther, S., Connell, J., Siochi, E., Harrison, J., Clair, S.T., 2002. Chem. Phys. Lett. 364, 303–310.
Rakhi, R.B., Sethupathi, K., Ramaprabhu, S., 2009. J. Phys. Chem. B 113, 3190–3194.
Reilly, C.A., Aust, S.D., 1997. Chem. Res. Toxicol. 10, 328–334.
Rodriguez-Lopez, J.N., Lowe, D.J., Hernandez-Ruiz, J., Hiner, A.N.P., Garcia-Canovas, F., Thorneley, R.N.F., 2001. J. Am. Chem. Soc. 123, 11838–11847.
Rubianes, M.D., Rivas, G.A., 2009. Electrochem. Commun. 5, 689–694.
Shu, F.R., Wilson, G.S., 1976. Anal. Chem. 48, 1679–1686.
Tsai, Y.-C., Li, S.-C., Chen, J.-M., 2005. Langmuir 21, 3653–3658.
Wang, J., 2008. Chem. Rev. 108, 814–825.
Wang, J., Li, M., Shi, Z., Li, N., Gu, Z., 2002. Anal. Chem. 74, 1993–1997.
Wang, J., Liu, G., Jan, M.R., 2004a. J. Am. Chem. Soc. 126, 3010–3011.
Wang, Z., Liang, Z., Wang, B., Zhang, C., Kramer, L., 2004b. Composites: Part A 35, 1225–1232.
Yao, Y.-L., Shiu, K.-K., 2008. Electroanalysis 20, 2090–2095.
Zeng, Y.-L., Huang, Y.-F., Jiang, J.-H., Zhang, X.-B., Tang, C.-R., Shen, G.-L., Yu, R.-Q., 2007. Electrochem. Commun. 9, 185–190.
Zengin, H., Zhou, W., Jin, J., Czerw, R., Smith, J.D.W., Echegoyen, L., Carroll, D.L., Foulger, S.H., Ballato, J., 2002. Adv. Mater. 14, 1480–1483.
Zhang, M., Smith, A., Gorski, W., 2004. Anal. Chem. 76, 5045–5050.
Zhao, X., Mai, Z., Kang, X., Zou, X., 2008. Biosens. Bioelectron. 23, 1032–1038.
Zhu, L., Yang, R., Zhai, J., Tian, C., 2007. Biosens. Bioelectron. 23, 528–535.
Zhu, L., Zhai, J., Guo, Y., Tian, C., Yang, R., 2006. Electroanalysis 18, 1842–1846.
Zhu, W., Zheng, J.P., Liang, R., Wang, B., Zhang, C., Walsh, S., Au, G., Plichta, E.J., 2008. ESC Trans. 16, 1615–1626.